

Scaling and Instabilities in Bubble Pinch-Off

J. C. Burton, R. Waldrep, and P. Taborek

Department of Physics and Astronomy, University of California, Irvine, California 92697, USA
(Received 12 August 2004; revised manuscript received 19 January 2005; published 11 May 2005)

We have used a 100 000 frame-per-second video to analyze the pinch-off of nitrogen gas bubbles in fluids with a wide range of viscosity. If the external fluid is highly viscous ($\eta_{\text{ext}} > 100$ cP), the bubble neck radius is proportional to the time before break, τ , and decreases smoothly to zero. If the external fluid has low viscosity ($\eta_{\text{ext}} < 10$ cP), the radius scales as $\tau^{1/2}$ until an instability develops in the gas bubble, which causes the neck to rupture and tear apart. Finally, if the viscosity of the external fluid is in an intermediate range, an elongated thread is formed, which breaks apart into micron-sized bubbles.

DOI: 10.1103/PhysRevLett.94.184502

PACS numbers: 47.55.Dz, 47.20.Cq, 47.20.Dr

There has been considerable recent interest in describing the generic features of the pinch-off process in fluids in which a single drop breaks into two disconnected pieces. Most work has been concerned with drops of a dense fluid such as water [1], glycerin [2], or mercury [3] immersed in a background fluid (usually air) of negligible density. In this case, there are two basic types of behavior that depend on the viscosity of the fluid drop: If the viscosity is negligible, the fluid filament that connects the separating droplets is conical in shape and the minimum neck radius is described by a $\tau^{2/3}$ power law, where τ is the time before separation. If the drop viscosity is large, the connecting fluid filament is nearly cylindrical with a radius that is linear in τ . Both the power laws and the geometric shape of the fluid filaments are universal in the sense that they are independent of the exact values of the fluid properties and the details of the initial conditions leading to breakup of the drop. A more detailed classification of typical behaviors is shown in [4].

If the external fluid in which the droplet is embedded has appreciable viscosity, the dynamics of the background fluid can affect the pinch-off process. For example, Doshi *et al.* [5] have shown that, if water drops of low viscosity pinch off in a background of high viscosity oil, the dynamics of the fluid filament is not self-similar, and the process is nonuniversal. Even if both the droplet and the external fluid have zero viscosity, numerical simulations suggest that the hydrodynamic stability of pinch-off flows is a sensitive function of the density ratio of the two fluids [6].

In this Letter we use high-speed video microscopy to investigate pinch-off of gas bubbles embedded in various background fluids with a range of viscosities. In bubble pinch-off, the roles of the high and low density fluids are reversed with respect to conventional liquid droplet pinch-off, and, although the governing equations are similar in both cases, the flow patterns and power laws that describe the evolution of pinch-off are distinctly different. Figure 1 contrasts the shape of the pinch region for an air bubble in water and a water droplet in air. The pinch region in gas bubbles has the local shape of a cylinder of revolution, with approximate rotational symmetry about the z axis as well

as reflection symmetry perpendicular to this axis at the narrowest point. A water drop pinching off in air, on the other hand, looks locally like a cone piercing a plate, and there is no reflection symmetry perpendicular to the rotational axis. If the external fluid has a high viscosity, the neck of a pinching bubble has a parabolic shape with a minimum neck radius that decreases linearly in time. For intermediate external viscosities, the bubble shape can produce elongated threads similar to those seen in Doshi *et al.* [5] using two liquids. For low viscosity background fluids, the bubble neck radius scales as $\tau^{1/2}$ until an instability truncates the power law collapse to zero neck diameter. To our knowledge, this is the first observation of this instability.

The basic equation describing bubble dynamics near the pinch region is a cylindrical version of the general Rayleigh-Plesset equation [7,8]:

$$\frac{P(r) - P_B}{\rho_{\text{ext}}} = (\ddot{R}R + \dot{R}^2) \ln \frac{R}{r} + \frac{1}{2} \dot{R}^2 - \frac{2\eta_{\text{ext}} \dot{R} + \sigma}{\rho_{\text{ext}} R}, \quad (1)$$

where R is the radius of the bubble, σ is the surface tension, η_{ext} and ρ_{ext} are the viscosity and density of the

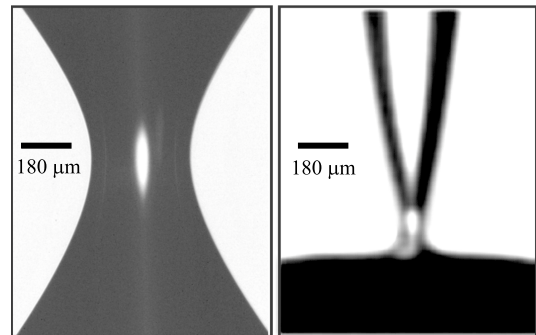


FIG. 1. Pinch-off in water-air systems showing the difference in the symmetry. In both cases, the interior fluid is dark with a light area in the center due to lensing of the illumination. On the left is an air bubble in water close to break-up whose shape is approximately a hyperboloid of revolution. On the right is a water droplet in air with the conical shape typical of inviscid self-similar pinch-off.

exterior fluid, and P_B and P_r are the pressures in the bubble and at some radius $r \gg R$, respectively. The derivation of this equation assumes that the external fluid flow is purely radial and has no vorticity so that the velocity can be described in terms of a potential. We ignore the rising motion of the bubble, characterized by a time scale of $(\eta_{\text{ext}}g/\Delta\rho)^{1/3}$, which is on the order of seconds and much larger than the few milliseconds required for pinch-off to occur. If we neglect the pressure in the bubble and assume a power law solution in time, $R = A(t_c - t)^\alpha$, then there are only two values of α that yield consistent asymptotic balances: $\alpha = 1/2$ or 1. When $\alpha = 1/2$, the logarithmic term is identically zero so $\ddot{R}R$ balances with \dot{R}^2 , regardless of the choice of A . When $\alpha = 1$, the most divergent parts of the equation are the surface tension and viscous terms, which are in balance when $A = \sigma/2\eta_{\text{ext}}$. When $\rho_{\text{int}}/\rho_{\text{ext}} \gg 1$, the interior flow cannot be neglected and the equation is no longer valid, especially since the reflection symmetry about the z axis is broken (Fig. 1). In this regime, one would expect $\alpha = 1$ for the viscosity dominated flows and $\alpha = 2/3$ for potential flow, as observed in numerous experiments and simulations [1,2,6,9–13].

The bubbles in our experiment consisted of pure nitrogen gas (viscosity = 0.018 cP). The fluids that we used included acetone (0.3 cP), water-glycerin mixtures (0.9–1011 cP), canola oil (72 cP), light corn syrup (2500 cP), and N4000 viscosity standard (12 000 cP) [14]. The surface tensions of the liquids were measured by capillary rise, and all were found to be within a factor of 2 of the surface tension of water (≈ 72 dyn/cm), except for acetone, which has a surface tension of ≈ 23 dyn/cm at room tempera-

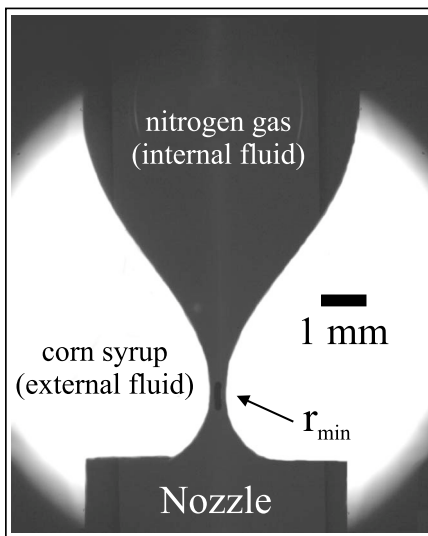


FIG. 2. A picture of a nitrogen bubble near pinch-off as it rises due to buoyancy in corn syrup. The illumination is from behind. The inner diameter of the nozzle is 3.2 mm. The outside fluid appears white while the bubble remains black. R_{min} is the minimum radius of the neck region of the bubble. Figure 3 shows a highly magnified view of this region.

ture. The experimental apparatus consisted of a 2-gallon aquarium tank filled with the appropriate fluid (corn syrup, water, etc.) and a glass or steel nozzle with an inner diameter of 3.2 mm placed 15 cm below the surface to deliver the bubbles (Fig. 2). A nitrogen gas line was connected to the nozzle through a mass flow controller so that the bubbling rate could be finely tuned. The aquarium tank was used to minimize the effects of the walls on the external fluid flow, so that we can assume the flow velocity is zero at infinity. The bubbles were produced at a rate of approximately one every five seconds. The imaging was done with an Infinity Research Phantom 7.0 digital video camera, capable of 100 000 fps at a 128×64 pixel resolution. The camera was attached to an adjustable bellows with a long focal distance microscope objective. The objective provided a resolution of $2.38 \mu\text{m}$ per pixel. The camera was triggered when the bubble began to pinch off, and the frame rate was chosen to match the speed of the breakup, which spanned several orders of magnitude depending on the viscosity of the fluids. Finally, the time evolution of the neck diameter and the curvature was extracted from the high-speed video by an edge-finding routine.

Figure 3 shows typical image sequences of the pinch-off of N_2 bubbles in several exterior fluids. Gas bubbles pinching in external fluids with viscosities ≥ 100 cP resemble Fig. 3(a), which shows nitrogen in glycerin. The bubbles have a cylindrical shape with a constant parabolic axial curvature, indicating a non-self-similar profile. The neck diameter continuously shrinks until the bubble separates into two pieces with sharply pointed ends. A more detailed numerical analysis of this type of behavior can be given by Suryo *et al.* [15]. For lower values of the external fluid viscosity (10–100 cP), there is a transition to a different flow regime represented by Fig. 3(b). The variation of R_{min} with time is no longer linear, and the axial curvature does not remain constant. As the neck radius approaches zero, its collapse is cut off by the formation of an elongated thread with a constant radius of $\approx 6 \mu\text{m}$, which is in good agreement with the scaling law described in [5] based on the ratio of internal to external viscosities. The thread persists for a surprisingly long time compared to the time it takes to collapse, and then eventually breaks up into ≈ 50 satellite bubbles due to the Rayleigh instability of a column of fluid. This type of non-self-similar pinch-off has been recently observed by Doshi *et al.* [5] using water drops immersed in high viscosity silicone oil. Figure 3(b) shows the first evidence of this type of flow in gas bubbles. For even lower values of the external viscosity (≤ 10 cP), we observed a transition to another flow regime, represented by Fig. 3(c), showing gas bubbles in water. Here, the axial curvature is more hyperbolic than parabolic, which has been previously predicted [16]. In contrast to the behavior at higher viscosities, the neck radius does not smoothly decrease to zero or a finite constant; rather, it undergoes a sudden rupture at a characteristic length scale of $R_{\text{min}} = 25 \mu\text{m}$ and a time scale of $10 \mu\text{s}$, as seen in

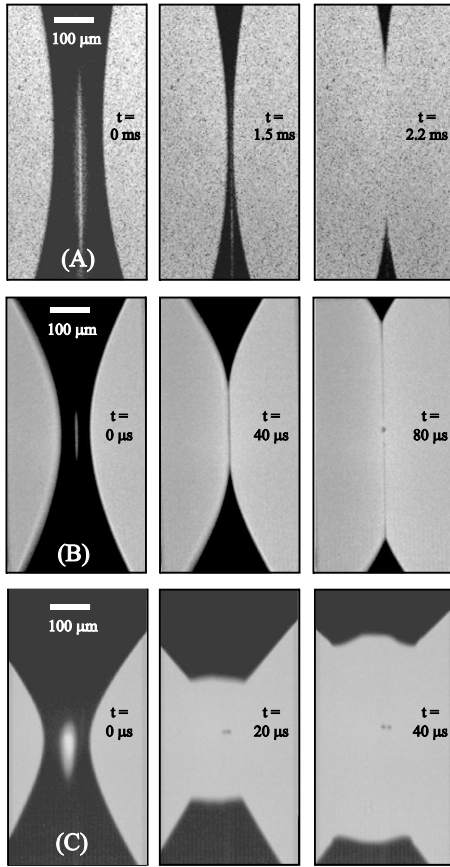


FIG. 3. The pinch-off of an interior fluid (dark) in an exterior fluid (light). (a) Nitrogen bubble in glycerin. This represents the generic behavior we observed for gas bubbles pinching in a high viscosity external fluid. The neck radius (R_{\min}) continually shrinks to zero with approximately constant axial curvature and then separates into two bubbles with cusplike ends. (b) Nitrogen bubble in 37.4 cP glycerin-water solution. As the bubble collapses, the two disjointed pieces form a thread of gas between them, then the thread proceeds to break up into micron-sized bubbles. (c) The low viscosity of the external fluid leads to an instability, which causes the bubble to rupture into two pieces with ragged ends. Note the two small satellite bubbles which are formed in the process.

more detail in Fig. 4. The ratio of radial to axial curvatures at R_{\min} varies by less than a factor of 2 while τ changes by a factor of 100, which might suggest a self-similar flow. However, the truly asymptotic regime is masked by the instability. A robust feature of the rupture process is the formation of two satellite bubbles approximately $10 \mu\text{m}$ in diameter. We believe that this rupture is due to an instability in the interface between the gas and the liquid, similar to the Kelvin-Helmholtz instability. The pinch-off of one inviscid fluid inside another has been studied previously using numerical simulations [6]. The calculations show that, when the density ratio $\rho_{\text{ext}}/\rho_{\text{int}} > 6.2$, the solutions become unstable. For bubbles in conventional fluids, $\rho_{\text{ext}}/\rho_{\text{int}} \approx 1000$, so pinch-off flows for bubbles in an inviscid external fluid are expected to be strongly unstable.

The three pinch-off mechanisms depicted in Fig. 3 can also be distinguished by their characteristic behaviors of R_{\min} vs τ . A plot of the neck diameter as a function of $\tau = (t_c - t)$ for three representative external fluids is shown in Fig. 5. For the low viscosities, t_c was bracketed by the video frame when the neck was connected, and the next frame when the bubble had ruptured and separated, giving an uncertainty of $\pm 5 \mu\text{s}$. For videos where elongated threads of gas appeared, t_c was chosen to be the time when the neck radius became constant ($\approx 6 \mu\text{m}$), since the flow after this point is determined by different dynamics [5]. In the high viscosity limit, t_c was chosen to be the point at which the two cusps separated.

Gas bubbles in high viscosity fluids have a neck that shrinks linearly in time due to a balance of surface tension and viscosity. R_{\min} is given by $(\sigma/2\eta_{\text{ext}})\tau$, where the prefactor is determined by Eq. (1) and has no adjustable parameters. The plot of this function in Fig. 5 shows that it agrees with the experimental data for glycerin to within a few percent. In the inviscid limit, the inertial terms in Eq. (1) dominate the flow and R_{\min} scales as $(L\sigma/\rho_{\text{ext}})^{1/4}\tau^{1/2}$, where L is the nozzle radius. The prefactor here is determined by dimensional considerations up to an overall dimensionless constant. The experimental data for water is accurately described by choosing a value of 1.22 for the constant, as shown in Fig. 5. The $\tau^{1/2}$ scaling of R_{\min} for bubbles in water has been observed [16,17] and predicted [7,16] previously, although those measurements

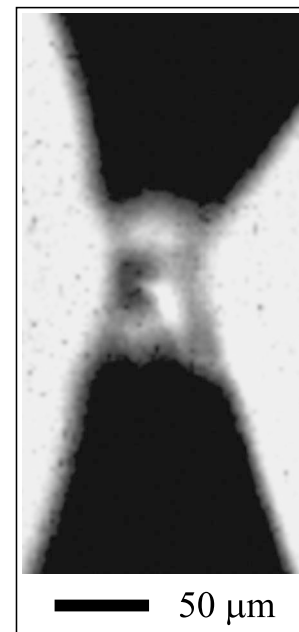


FIG. 4. N_2 bubble in water at the moment of rupture. The speed of the video was 100 000 fps and the exposure time was $2 \mu\text{s}$. The dark areas are gas and the lighter areas are water. Because of the focusing of the light in the center and the lack of resolution ($128 \text{ pixels} \times 64 \text{ pixels}$), it is difficult to distinguish between gas and liquid.

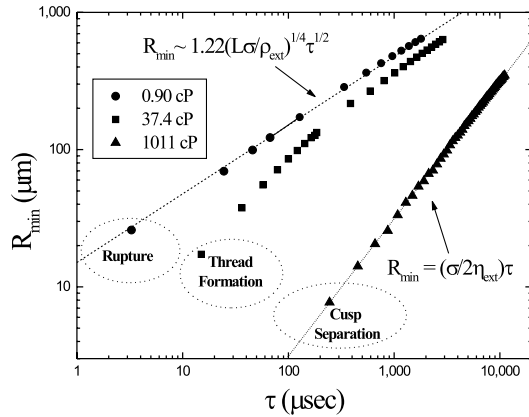


FIG. 5. Log-log plot of the minimum neck radius vs τ (time before the pinch) for bubbles in three representative fluids: circles, water; squares, water-glycerin; triangles, pure glycerin. Each curve corresponds to one of the sequences of pictures in Fig. 3. When the external flow was in the inertial regime (low viscosity limit), the neck radius followed a $(\tau^{1/2})$ scaling law. In the Stokes flow regime (high viscosity limit), the neck radius followed a linear scaling law. The derivation of the prefactor for each of these cases is given in the text. The type of final pinch-off corresponding to each curve is indicated by the text at the short time end point.

were limited to $\tau > 2$ ms and could not resolve features such as the rupture seen in Fig. 4. For values of the external fluid viscosity between 10 and 100 cP, R_{\min} scales with τ with an exponent between $1/2$ and 1.

To investigate the power law dependence between R_{\min} and τ as a function of viscosity, we fitted all data below $R_{\min} = 200 \mu\text{m}$ to a power law model ($R_{\min} = A\tau^\alpha$), and plotted α as a function of viscosity (Fig. 6). The transition from $\alpha = 1/2$ to 1 occurs in a surprisingly narrow regime, which is associated with thread formation. Also, it is noteworthy that data obtained from fluids with viscosities varying over 5 orders of magnitude and surface tensions varying by a factor of 2 lie on a smooth continuous curve.

In conclusion, we have seen three basic types of flow behavior in bubble pinch-off. Bubbles in viscous fluids ($\eta_{\text{ext}} > 100$ cP) collapse linearly in time, until the neck radius reaches dimensions beyond optical resolution. Bubbles in fluids with a rather narrow intermediate range of viscosities (10–100 cP) produce long, thin threads of gas of constant radius. Finally, bubbles in low viscosity fluids ($\eta_{\text{ext}} < 10$ cP), such as water, follow a $\tau^{1/2}$ power law until the shear between the interior and exterior flows causes an instability that leads to the rupture of the bubble. The dynamics of rupture is remarkably fast; the neck profile evolves from a smooth hyperboloid of revolution to two truncated cones with ragged edges within $10 \mu\text{s}$. Both characteristic power laws are asymptotic solutions to the Rayleigh-Plesset equation for cylindrical bubbles. In all the flow regimes, the neck region is a cylinder of revolution with reflection symmetry. Although previous numerical work has identified an instability in the self-similar solu-

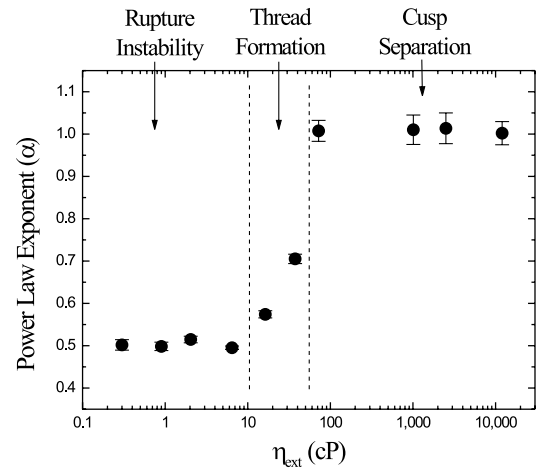


FIG. 6. Semi-log plot of the fitted power law exponent vs η_{ext} for bubbles in fluids of varying viscosity. The measurements were taken for flows where $R_{\min} < 200 \mu\text{m}$, and were fitted using the model $R_{\min} = A(t_c - t)^\alpha$. Between 10 and 100 cP, the exponent has a transition from $\alpha = 1/2$ to 1.

tion with $R_{\min} \sim \tau^{2/3}$ [6], the instability observed in the experiments seems to be an instability of the $R_{\min} \sim \tau^{1/2}$ solution.

This work was supported by NASA NAG8-1437 and NSF DMR 9971519.

- [1] A. U. Chen, P. K. Notz, and O. A. Basaran, *Phys. Rev. Lett.* **88**, 174501 (2002).
- [2] X. D. Shi, M. P. Brenner, and S. R. Nagel, *Science* **265**, 219 (1994).
- [3] J. C. Burton, J. E. Rutledge, and P. Taborek, *Phys. Rev. Lett.* **92**, 244505 (2004).
- [4] I. Cohen and S. R. Nagel, *Phys. Fluids* **13**, 3533 (2001).
- [5] P. Doshi, I. Cohen, W. W. Zhang, M. Siegel, P. Howell, O. Basaran, and S. R. Nagel, *Science* **302**, 1185 (2003).
- [6] D. Leppinen and J. R. Lister, *Phys. Fluids* **15**, 568 (2003).
- [7] H. N. Oğuz and A. Prosperetti, *J. Fluid Mech.* **257**, 111 (1993).
- [8] M. S. Plesset and A. Prosperetti, *Annu. Rev. Fluid Mech.* **9**, 145 (1977).
- [9] R. F. Day, E. J. Hinch, and J. R. Lister, *Phys. Rev. Lett.* **80**, 704 (1998).
- [10] Y. J. Chen and P. H. Steen, *J. Fluid Mech.* **341**, 245 (1997).
- [11] E. D. Wilkes, S. D. Phillips, and O. A. Basaran, *Phys. Fluids* **11**, 3577 (1999).
- [12] I. Cohen, M. P. Brenner, J. Eggers, and S. R. Nagel, *Phys. Rev. Lett.* **83**, 1147 (1999).
- [13] J. Eggers, *Phys. Fluids* **7**, 941 (1995).
- [14] *CRC Handbook of Chemistry and Physics*, edited by D. R. Lide (CRC Press, Boca Raton, FL, 2004), 84th ed.
- [15] R. Suryo, P. Doshi, and O. A. Basaran, *Phys. Fluids* **16**, 4177 (2004).
- [16] M. S. Longuet-Higgins, B. R. Kerman, and K. Lunde, *J. Fluid Mech.* **230**, 365 (1991).
- [17] D. Lohse (private communication).